ProSafeNet

International Journal of Disaster Risk Management • Vol. 7, No. 2 • https://doi.org/10.18485/ijdrm.2025.7.2.1

Publisher: Scientific-Professional Society for Disaster Risk Management

International Journal of Disaster Risk Management

Article

Advanced Flood Risk Mapping in Bouarfa Watershed Using Integrated Machine Learning, GIS, and MCDM

Alioua Zahar Elkheir[1*], Mezrhab Abdelhamid[1], Laaboudi Mohammed[1], Achebour Ali[1], Sahil Mohammed[1], Elyagoubi Said[1], Melhaoui Mohammed[1]

[1] Geographic Information Technology and Spatial Management Team, Communication, Education, Digital Use and Creativity Laboratory, Faculty of Arts and Humanities, Mohammed Premier University Oujda

* Corresponding: zaharelkheir.alioua.d24@ump.ac.ma

Received: 13 August 2025; Revised: 3 October 2025; Accepted: 01 November 2025; Published: 30 December 2025.

ABSTRACT

In Morocco, floods occur frequently, often causing significant damage to infrastructure and the environment due to a lack of adequate protective measures. The unpredictability of these events is attributable to climate change and the irregular nature of weather conditions. However, determining flood susceptibility can facilitate the mitigation and prevention of risk. This study aims at mapping flood-susceptible areas in the Bouarfa watershed using a multi-criteria decision analysis (MCDA) approach integrated within a Geographic Information System (GIS). Seven key conditioning parameters were considered: altitude, slope, geology, drainage density, flow accumulation, land use/land cover (LULC), and soil. The Analytical Hierarchy Process (AHP) was used to assign weights to these factors. The results obtained demonstrate that 39.53% (546.24 km^2) of the territory is exposed to a very low to moderate flood risk and 60.47% (835.59 km^2) to a high to very high flood risk. The model's accuracy was validated using historical flood locations and the Area Under the Curve (AUC) method, which yielded a value of 84.5%, indicating very good performance. This map serves as a critical tool for decision-makers for risk mitigation and land-use planning in this arid region.

KEYWORDS

Hierarchy analytical process (ahp); flood susceptibility; multi-criteria decision making (mcdm); vulnerability; bouarfa watershed.

Elkheir, A. Z., Abdelhamid, M., Mohammed, L., Ali, A., Mohammed, S., Said, E., & Mohammed, M. (2025). Advanced Flood Risk Mapping in Bouarfa Watershed Using Integrated Machine Learning, GIS, and MCDM. International Journal of Disaster Risk Management, 7(2), 1–20. Retrieved from https://internationaljournalofdisasterriskmanagement.com/index.php/Vol1/article/view/216

1. Introduction

Both rich and developing countries confront natural disasters, causing major material losses, costly economic disruption, and severe human suffering. Among these, floods are the most prevalent and destructive, occurring with alarming frequency across the globe (Das, 2018; Doocy et al., 2013). Floods are defined as the overflow of water that results in the submersion of land, leading to the destruction of infrastructure, urban areas, and agricultural land, often with tragic loss of life and severe economic consequences (Dewan, 2013; Merz et al., 2010). Climate is a primary factor influencing the occurrence and evolution of floods, with climate change expected to alter land use and land cover (LULC), thereby increasing flood risk (Emerton et al., 2017).

In recent decades, remote sensing and Geographic Information Systems (GIS) have become indispensable tools for mapping flood vulnerability and analyzing natural hazards (Bates, 2012; Pradhan et al., 2009). Various geospatial techniques have been applied, which can be broadly classified into three categories: (1) hydrological models like SWAT (Oeurng et al., 2011); (2) machine learning techniques such as Artificial Neural Networks (ANN) (Kia et al., 2012) and Support Vector Machines (SVM) (Tehrany et al., 2015); and (3) statistical methods like Weights of Evidence (WoE) and Logistic Regression (LR) (Rahmati et al., 2016). Alongside these, Multi-Criteria Decision Making (MCDM) methods, particularly the Analytical Hierarchy Process (AHP), have gained prominence for their ability to integrate diverse factors and expert knowledge into a structured framework (Das, 2018; Kazakis et al., 2015).

While numerous studies have applied these techniques globally, there remains a research gap in their application to the specific arid and semi-arid environments of southeastern Morocco, which are characterized by infrequent but intense rainfall events leading to destructive flash floods. Previous flood studies in Morocco have often focused on more humid coastal or mountainous regions or have used different methodological approaches. This study aims to fill this gap by developing a detailed flood susceptibility map for Bouarfa watershed. The primary objective is to delineate flood-prone areas by integrating seven critical geo-environmental factors using a combined GIS and AHP-based MCDM methodology. The novelty of this research lies in the specific application and validation of this integrated model in a data-scarce, arid region, providing a tailored and robust tool for regional-scale flood risk management and land-use planning.

The findings of this study are intended to facilitate informed decision-making, thereby minimizing potential flood-related damage and financial losses. The feasibility of this work was supported by the availability of datasets such as ASTER-DEM, Sentinel-2 imagery, and soil and geological maps, all processed to a 10-meter resolution.

2. Study area

The study area is Bouarfa watershed, which is susceptible to flooding from the rivers that traverse it. The town of Bouarfa is located in southeastern Morocco, 40 km from the country’s southern border and 60 km from the eastern border, at an altitude of 1150 m, on the southern slopes of Jbel Bouarfa (1850 m) and the Hezem El Ahmar relief (Fig. 1). This renders the town vulnerable to flooding from the rivers that traverse it, as well as to floodwater from the chaâbas, which serve to drain rainwater and subsequently discharge it into the town.

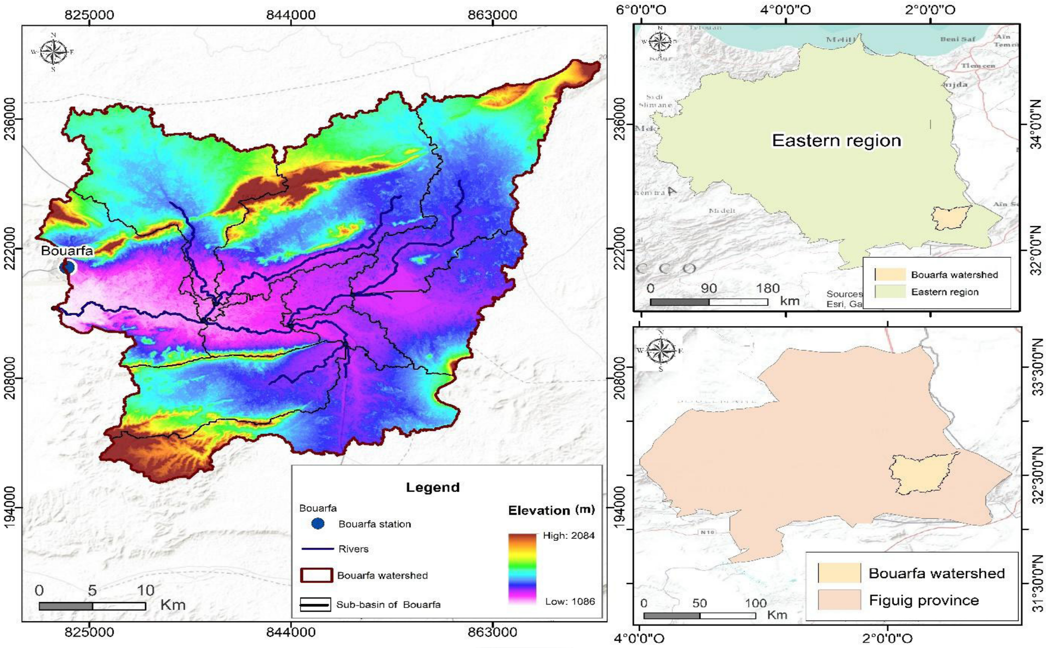

Figure 1. Map of the topography of Oued Bouarfa basin

The watershed under scrutiny in this study is characterised by a relatively dense hydrographic network. The catchment area is comprised of multiple sub-watersheds of varying sizes and morphologies, including Oued Chegga, Oued Chegga, and Oued Chegga aval. Oued Bouarfa constitutes the primary collector, receiving numerous tributaries in the process. Furthermore, Bouarfa catchment area is susceptible to flooding, with the potential for significant damage in the event of torrential rainfall. The floods are attributed to natural factors, including the topographical and hydrological characteristics of the surrounding relief, the presence of numerous wadis and chaâbas within the urban area, and the city's highly irregular climate.

The Bouarfa basin is distinguished by a continental climate that is markedly arid, with a particularly hot and dry summer season and a very cold winter. The climate is classified as quasi-Saharan, with a marked scarcity of rainfall. As is typical of this geographical region, precipitation is generally limited and sporadic. The average annual rainfall currently exhibits a fluctuation between 145 mm and 190 mm (Fig. 2).

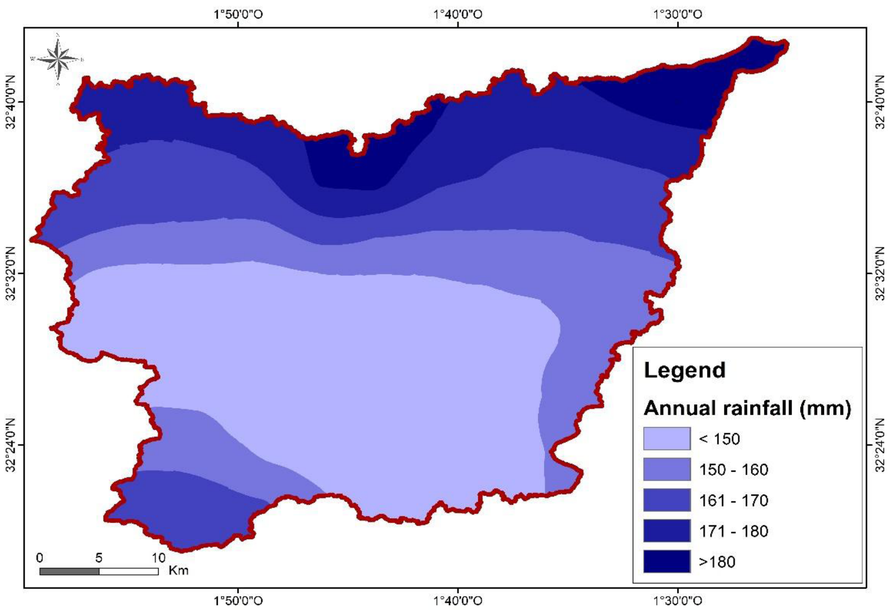

Figure 2. Map of the average annual precipitation in Oued Bouarfa basin from 1981 to 2022

3. Geospatial layers for flood vulnerability mapping

The selection of flood conditioning factors is a critical step in flood susceptibility mapping (FSM). While there is no universal consensus on the number or type of factors, most studies recommend using a comprehensive set to avoid bias (Mahmoud & Gan, 2018). For this study, seven conditioning factors were selected based on their established influence on flood occurrence and data availability. The two most controversial issues in FSM research are the number of flood conditioning factors and which factors should be selected to provide flood protection (Vojtek & Vojteková, 2019). For this study, seven conditioning factors were selected in a manner similar to the ones used in other FSM experiments conducted elsewhere (Elkhrachy, 2015; Kazakis et al., 2015). However, other studies have selected four parameters (Kourgialas & Karatzas, 2011; Rahmati et al., 2016) or six factors (Samanta et al., 2016). Furthermore, studies have used ten, eleven and twelve factors (Choubin et al., 2019; Haghizadeh et al., 2017; Khosravi et al., 2016; Zhao et al., 2018). It is generally advisable, however, to include more than six factors in order to avoid a single weight dominating the others and increasing the risk of some components being overvalued (Mahmoud & Gan, 2018).

The seven key factors were selected for this study: altitude, slope, geology, drainage density, flow accumulation, land use/land cover (LULC) and soil. These factors were chosen for several reasons. First, they are widely recognized in the literature as primary controls on hydrological processes in arid and semi-arid landscapes (Das, 2018; Kazakis et al., 2015). Second, reliable data for these factors were available for Bouarfa watershed from sources like ASTER-DEM and Sentinel-2.

Factors such as precipitation intensity were not included as a direct layer because the study focuses on mapping inherent susceptibility based on the watershed's static physical characteristics, rather than modeling a specific rainfall event. Similarly, while NDVI is useful, LULC provides a more direct classification of surface types (e.g., built-up areas, bare soil) that directly influence runoff. Each of these seven factors was reclassified into five classes using the equal-interval method in ArcGIS and is presented in Figure 3.

3.1. Topographical slope

Slope is a key topographic factor that strongly influences surface runoff, infiltration, and water retention. Gentle slopes tend to accumulate water, making them more susceptible to flooding, whereas steep slopes facilitate rapid runoff (Das, 2018). As demonstrated by Das & Pardeshi (2018), runoff velocity on steep terrain is inversely proportional to the rate of soil infiltration. Consequently, low-lying areas are more exposed to flooding due to the stagnation of large water volumes (Li et al., 2012; Pradhan et al., 2009).

The influence of slope on hydrological behavior is therefore a crucial determinant of flood vulnerability. Numerous studies have confirmed a direct correlation between slope gradient and runoff velocity (Fernández & Lutz, 2010; Tehrany et al., 2013; Youssef et al., 2011). The slope map (Figure 3A) was produced in the ArcGIS environment using data from the ASTER DEM.

3.2. Geology

The underlying geology plays a crucial role in controlling surface runoff through the permeability of rock formations. Impermeable layers enhance runoff and increase flood risk (Bonacci et al., 2006), whereas permeable lithological units promote infiltration and reduce the likelihood of flooding. A strong correlation has been demonstrated between rock permeability and infiltration rate (Bonacci et al., 2006). According to Reneau (2000), specific geological features can significantly influence runoff dynamics and flood occurrence, a relationship also highlighted by Kazakis et al. (2015).

The geology of Bouarfa watershed is predominantly sedimentary, ranging in age from the Jurassic to the Pleistocene, and composed mainly of carbonate formations with variable permeability

(Fig. 3B). Bouarfa High Atlas is characterized by the extensive Tamlelt Plain an outcrop of the Lower Paleozoic basement covering approximately 2000 km².

The Jurassic series consists mainly of alternating marl and limestone beds, which are especially prominent east of Bouarfa meridian. These strata, thick and becoming increasingly calcareous towards the top, correspond to the Upper Bajocian and Lower Bathonian. To the east, the Jurassic continues with detrital facies of pink sandstone containing fossilized wood, interbedded with pelitic and reefal levels that attest to the proximity of land during deposition.

The Cretaceous series rests unconformably on the Jurassic and appears on the northern and southern flanks of the eastern Atlas, as well as in two small synclines southeast of Tamlelt Plain. In Bouarfa, this sequence begins with conglomerates overlain by red sandstones, followed by limestone horizons and the marly Cenomanian series. The geology of the region is further marked by a prominent ledge of Turonian limestone, typically white and occasionally flinty in texture. Finally, the sequence is capped by a substantial detrital unit about 100 meters thick, composed of pink sandstones and conglomerates assigned to the Senonian period.

3.3. Flow accumulation

Flow accumulation represents the volume of upstream water flowing into each pixel, identifying areas where surface runoff is likely to concentrate and, consequently, where flooding is more probable (Kazakis et al., 2015; Lehner et al., 2006; Mahmoud & Gan, 2018). This layer (Fig. 3E), derived from the ASTER-DEM, serves as a key conditioning factor in hydrological and flood susceptibility modeling (FSM) studies. Conceptually, flow accumulation denotes the aggregation of a pixel's flow from adjacent pixels, thus delineating zones of concentrated surface runoff. In this study, after determining flow directions, the flow accumulation command in the ArcGIS environment was applied to generate the flow accumulation layer from the ASTER-DEM.

3.4. Land use and occupation (LULC)

Surface cover plays a crucial role in influencing flood probability, as impervious surfaces such as built-up areas and bare land tend to increase runoff, whereas vegetated zones mitigate it (Benito et al., 2010; Chapi et al., 2017; García-Ruiz et al., 2013; Norman et al., 2010). The Land Use and Land Cover (LULC) map (Fig. 3F), derived from Sentinel-2 imagery, comprises six classes: shrubland, grassland, cropland, built-up areas, sparse or bare vegetation, and permanent water bodies (Table 1), with the area being predominantly covered by bare or sparse vegetation (87.51%).

As emphasized in previous studies, LULC constitutes a key determinant in identifying zones with a high propensity for flooding, since surface cover and land use changes over time directly affect runoff dynamics and flood susceptibility. In this study, the Sentinel-2 dataset was therefore employed to generate the LULC layer, providing essential input for assessing the spatial variability of flood risk.

Table 1. Percentage distribution of LULC classes in the Bouarfa Watershed

S. No	LULC category	Area in km²	LULC Classes (%)
1	Bare / Sparse Vegetation	1226.09	87.51
2	Built up	0.97	0.07
3	Cropland	6.61	0.47
4	Grassland	166.55	11.89
5	Permanent Water Bodies	0.19	0.01
6	Shrubland	0.62	0.04

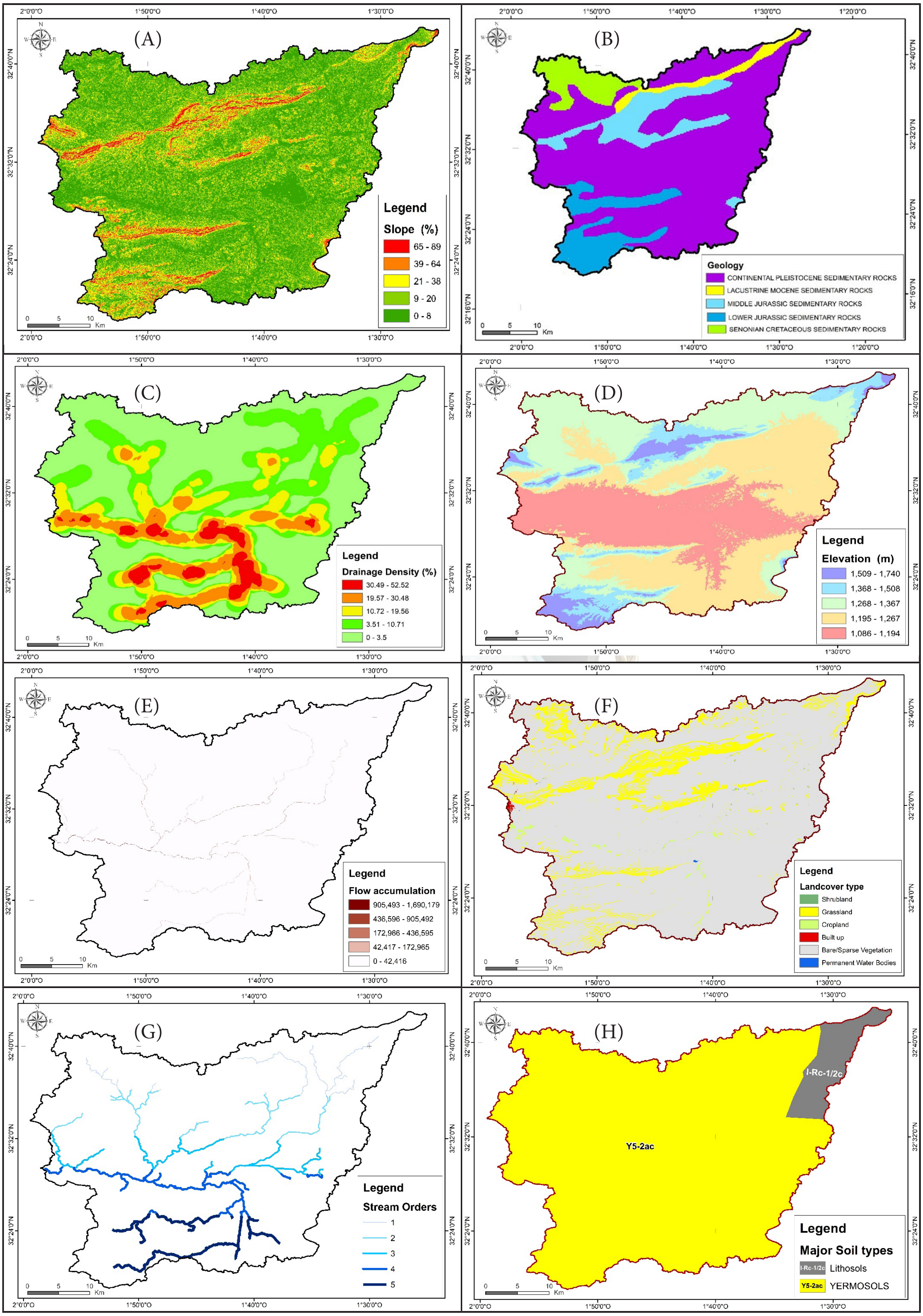

Figure 3. The flood conditioning factors (a) slope, (b) geology, (E) Flow accumulation, (F) land use/cover, (C) Drainage density (D) Elevation (G) stream order (H) Soil.

3.5. Drainage density

Drainage density, defined as the total length of streams per unit area, is strongly correlated with flood occurrence, as high drainage density reflects efficient and rapid runoff, thereby increasing flood potential (Kumar et al., 2015; Gül, 2013). The drainage density map (Fig. 3C), derived from the ASTER-DEM, was generated using the drainage network and the linear density tool in the ArcGIS environment to quantify drainage density values. A quantile classification method was then applied to divide the map into five distinct classes, providing a spatial representation of areas with varying susceptibility to flooding based on the distribution of drainage density.

3.6. Altitude

Elevation is a primary factor controlling the direction, movement, and depth of floodwaters, as low-lying areas are naturally more susceptible to inundation due to water flowing from higher to lower elevations (Botzen et al., 2013; Dahri & Abida, 2017; Das, 2018; Stieglitz et al., 1997). The elevation map (Fig. 3D), derived from the ASTER-DEM, was classified using the ArcGIS surface analysis tool with an equal interval scale into five classes, representing different elevation ranges, to illustrate areas with varying susceptibility to flooding.

3.7. The nature of the soil

Soil type significantly influences flooding through its permeability, as sandy soils with high permeability facilitate infiltration, while clayey soils with low permeability promote surface runoff (Ibrahim-Bathis & Ahmed, 2016). In the study area, two main soil types are present: calcimagnesic soils and poorly developed erosion soils, with lithosols exhibiting greater mass compared to yermosols (Fig. 3H). The variation in soil type and texture directly affects the capacity of water to infiltrate the ground, making soil characteristics a critical factor in flood occurrence and the effective management of water resources.

4. Methodological approach

The methodology for this study is illustrated in Figure 4. It involves three main stages: (1) data collection and preparation, (2) application of the AHP model to determine factor weights, and (3) generation and validation of the flood susceptibility map.

4.1. Analytical Hierarchy Process (AHP)

The AHP, developed by Saaty (1977), is a widely used MCDM technique for assigning weights to criteria based on their relative importance. The process involves creating a pairwise comparison matrix where each factor is compared against every other factor using a scale from 1 (equal importance) to 9 (extreme importance). In this study, the pairwise comparison was based on a comprehensive literature review and expert judgment regarding the influence of each factor on flooding in arid environments. The consistency of these judgments is verified by calculating the Consistency Ratio (CR). A CR value of less than 0.10 indicates that the judgments are consistent and the derived weights are reliable.

4.2. Weight of factors

The MCDA method is a valuable tool for evaluating geospatial datasets, as it enables the determination of their respective influences (Adiat et al., 2012). In this study, AHP was identified as the most suitable MCDA approach through a comparative analysis of alternative methods (see Figure

4). As Malczeski (2006) asserts, the relative weights of conditioning components can be established in one of four ways.

a) The following section will provide a detailed overview of the most commonly used ranking methods. Each criterion is then assigned a ranking in accordance with the priorities established by the decision-maker. In order to accomplish this, it is necessary to compare each criterion with all the others.

b) With regard to the methods of scoring, these processes entail the estimation of weights through the utilization of a designated scale.

c) Pairwise comparison approaches: These techniques entail conducting direct trade-off analyses between different alternatives and performing pairwise comparisons with the objective of creating a ratio matrix.

d) Analyze trade-off techniques. These are based on direct comparisons of trade-offs between pairs of options.

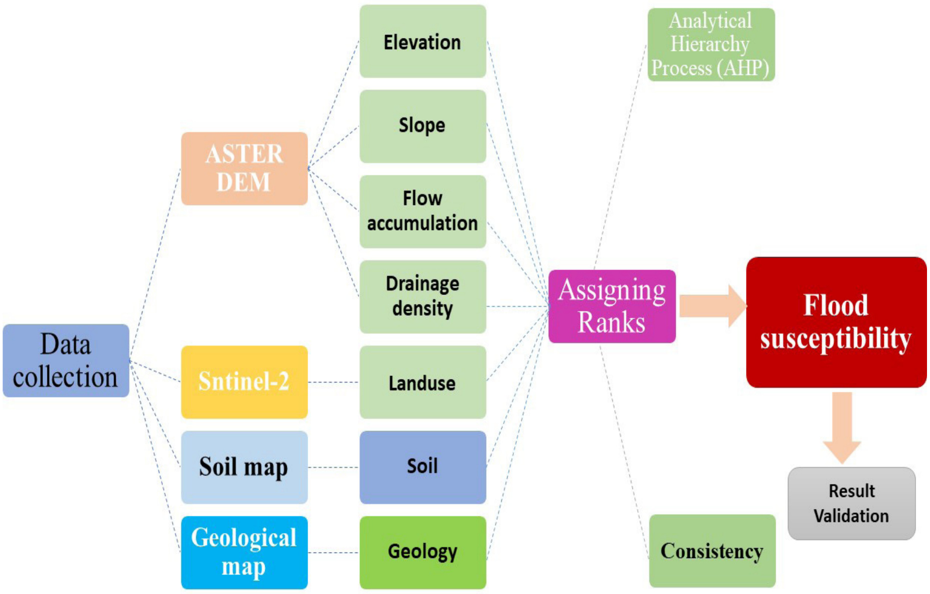

Figure 4. The flow diagram employed to perform flood susceptibility mapping in the ArcGIS environment.

The choice of the three-way comparison method for this study was motivated by its numerous advantages, including the provision of a structured framework for group discussions and the facilitation of the identification of areas of agreement and disagreement by decision-making teams when determining the weighting of criteria. The following steps constitute the AHP method: Saaty and Vargas (2012) propose a methodology for the enhancement of decision-making processes. The methodology involves the following steps:(a) The problem is decomposed into a series of constituent components (b) These components are then prioritized (c) Each component is assigned a numerical value according to its importance (d) A comparison matrix is created (e) The weight of each component is calculated using the normalized eigenvector. The present procedure facilitates the comparison of disparate components. The results obtained were assigned according to their proportional weight and influence (Table 2). The significance of the criterion in the overall calculation increases in proportion to the magnitude of the weight (Malczewski, 2006). Within the three-way comparison matrix, the rows correspond to the inverse score of each factor and the relationship between that factor and the other factors (see Table 3). Subsequently, the following formula is employed to construct a pair-wise comparison matrix, with normalized diagonal factors set at a value of 1.

$$A = (a_{ij})_{n*n} = \begin{bmatrix} a_{11} & a_{12} & \dots a_{1n} \\ a_{21} & a_{22} & \dots a_{2n} \\ a_{n1} & a_{n2} & \dots a_{nn} \end{bmatrix}, \ a_{ii} = 1, \ a_{ij} = \frac{1}{a_{ji}}, \ a_{ij} \neq 0 \tag{1}$$

Table 2. The fundamental scale of absolute numbers as modified after (Saaty, 1980)

Intensity of Importance	Definition	Explanation
1	Equally significant	The goal is equally benefited by the two activities.
2	Weak or slight	The scores of transition
3	Moderately more significant	One activity is marginally preferred over another based on experience and judgment.
4	Moderate plus	The scores of transition
5	Strongly more significant	One activity is greatly preferred over another by experience and judgment.
6	Strong plus	The scores of transition
7	Very strong more significant	A particularly strong preference for one activity over another is evident in practice.
8	Very, very strong more significant	The scores of transition
9	Extremely more significant	The strongest potential order of affirmation can be found in the evidence favoring one activity over another.

The application of the weighted arithmetic mean technique (see Table 4 and equation (2)) results in the standardization of the results of the pairwise comparisons, thereby creating the standard pairwise comparison matrix. The largest characteristic root can be expressed as follows:

$$Aw = \lambda maxw. \tag{2}$$

Table 3. Comparison matrix and the relative score of each factor

	1	2	3	4	5	6	7
1	1	1.00	2.00	3.00	4.00	5.00	6.00
2	1.00	1	2.00	3.00	4.00	5.00	6.00
3	0.50	0.50	1	2.00	3.00	4.00	5.00
4	0.33	0.33	0.50	1	2.00	3.00	4.00
5	0.25	0.25	0.33	0.50	1	2.00	3.00
6	0.20	0.20	0.25	0.33	0.50	1	2.00
7	0.17	0.17	0.20	0.25	0.33	0.50	1

Table 4. Normalized and the weight values in the standardized pairwise comparison matrix.

N°	Parameter	Weights assigned	Priority (%)	Rank
1	Elevation	0.287	27.8%	1
2	Slope	0.287	27.8%	1
3	Drainage Density	0.176	17.6%	2
4	LULC	0.114	11.4%	3
5	Soil	0.073	7.3%	4
6	Geology	0.048	4.8%	5
7	Flow accumulation	0.033	3.3%	6

Table 5. Sub-criteria for each parameter and weightings applied.

S. No	Parameters	Range of values	Ranks
1	**Elevation**	1086-1194 1195-1267 1268-1367 1368-1508 1509-1740	1 2 3 4 5
2	**Slopes**	0-8.06 8.06 - 19.71 19.71 - 37.63 37.63 - 63.62 63.62 - 228.51	1 2 3 4 5
3	**Drainage density**	29.85 - 50.75 19.90 - 29.85 11.34- 19.90 3.78 - 11.34 0 - 3.78	1 2 3 4 5
4	**Flow accumulation**	905.439-1690.179 436.596-905.492 172.966-436.595 42.471-172.965 0-42.416	1 2 3 4 5
5	**LULC**	Tree Cover Permanent Water Bodies Bare/Sparse Vegetation Built up Cropland Grassland	4 2 3 1 5 6
6	Geology	Sedimentary rocks (Senonian Cretace) Sedimentary rocks (Lower Jurassic) Sedimentary rocks (Middle Jurassic) Sedimentary rocks (Lacustrine Mocene) Sedimentary rocks (Continental Pleistocene)	2 5 4 3 1
7	**Soil type**	Lithosols Yermosols	1 2

In order to ascertain the optimal set of weights, it is necessary to calculate the principal vector of the pairwise comparison matrix (see Eq. 3). The following steps can be taken to obtain the closest approximation to this conclusion (Leake & Malczewski, 2000).

In order to calculate the mean of the values in each column of the comparison matrix, the values in each column must be added together.

- The normalized pair-wise comparison matrix is derived by dividing each element of the matrix by the sum of its columns. Then, the average of the entries in each row of the matrix obtained after calculation is determined.
- The subsequent step involves dividing the total normalized scores for each row by the total number of criteria to create the matrix.

These means are employed to estimate the relative weight of the relevant criteria. In this context, the weights are regarded as the mean of all potential methods of criteria comparison (see Table 5). According to Saaty (1980), the relationship signifies the consistency of the AHP technique.

$$CR = \frac{CI}{RI} \tag{3}$$

$$\text{Whereas : } CI = \frac{\lambda max - n}{n - 1} \tag{4}$$

Maximum likelihood estimation (MLE) is a statistical technique that is used to calculate the principal eigenmode of a given matrix. The total number of matrix components is denoted by n, the coherence ratio is represented by CR, the coherence index is denoted by CI, and the random index is denoted by RI. The number of factors in the comparison matrix is used to construct the coherence ratio, which is based on the RI values (Saaty, 1977, 1980). The pairwise comparison matrix is considered sufficiently accurate when the CR value is less than 0.10. As Saaty (1977) noted, if this value exceeds 0.10, the matrix is deemed inconsistent and necessitates recalibration. The consistency coefficient of 0.018 in our present study indicates a satisfactory level of consistency (see Table 3).

4.3. Flood Susceptibility Index (FSI)

The Flood Susceptibility Index (FSI) was calculated using the Weighted Linear Combination (WLC) method within the ArcGIS environment. This method consists of multiplying the weight of each factor by the rank of its corresponding class and summing the results for each pixel, as expressed by the following equation

$$FSI = \sum_{i=1}^{n} (wi \times ri) \tag{5}$$

Here, W_i represents the weight assigned to each parameter, while rir_iri corresponds to the parameter rating at each location; $_i$=1,2,…,ni = 1, 2, …, n_i=1,2,…,n, where nnn indicates the total number of parameters considered.

In the final stage of the analysis, all flood-conditioning factors were integrated, and their respective weights were applied to generate the Flood Susceptibility Index (FSI) map (Figure 1). The aggregated results produced a comprehensive flood susceptibility map, which was subsequently reclassified into five distinct categories: very low, low, moderate, high, and very high susceptibility zones.

5. Results and discussion

5.1. Flood Susceptibility Map

The final flood susceptibility map (Fig. 5) illustrates the spatial variability of flood risk across Bouarfa watershed. The analysis reveals that a large portion of the basin is highly exposed to flooding, with 21.01% (290.36 km²) of the total area exhibiting very high susceptibility and 39.46% (545.23 km²) classified as highly susceptible. In contrast, the areas of very low, low, and moderate susceptibility represent 10.35%, 12.18%, and 17.00% of the watershed, respectively (Table 6). These results emphasize that more than half of the study area (around 60%) is under significant flood risk, highlighting the critical importance of implementing effective flood management strategies.

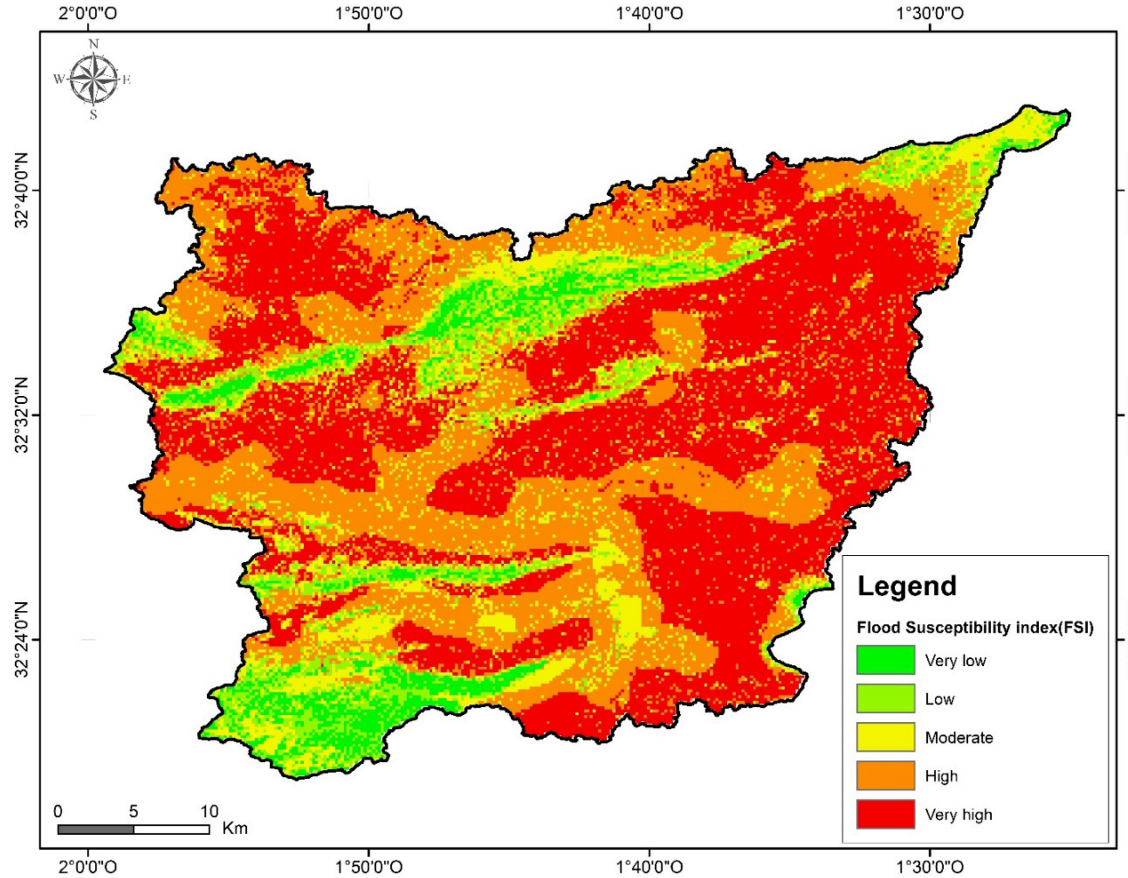

Figure 5. Flood susceptibility map of the study area based on AHP

Table 3. Distribution of flood susceptibility classes in the Bouarfa watershed

Susceptibility Class	Area (km²)	Area (%)
Very Low	143.03	10.35
Low	168.32	12.18
Moderate	234.89	17.00
High	545.23	39.46
Very High	290.36	21.01
Total	**1381.83**	**100**

As shown in Figure 5, the flood vulnerability analysis further confirms this trend, indicating that 36.05% (498.1 km²) of the basin faces very high flood risk, 56.09% (775.14 km²) falls under moderate risk, and only 7.86% (108.59 km²) is considered low risk. The highest susceptibility is concentrated in the central and downstream portions of the watershed, particularly in areas characterized by low elevation, gentle slopes (0–5°), and endoreic drainage patterns. These conditions promote water accumulation and reduce runoff velocity, leading to a higher likelihood of surface flooding. Moreover, these flood-prone areas often coincide with Quaternary alluvial deposits that, although permeable, can become saturated during heavy rainfall events. The high drainage density and pronounced flow accumulation in the valley bottoms further exacerbate flood hazards.

In contrast, the regions exhibiting low susceptibility are primarily located in the northern and southern highlands of the watershed, where steep slopes and higher elevations encourage rapid water drainage, minimizing flood potential. The city of Bouarfa, situated within a high-susceptibility zone, remains particularly vulnerable, emphasizing the urgent need for adaptive urban planning and flood mitigation measures to safeguard infrastructure and populations in at-risk areas.

5.2. Validation of the flood susceptibility map

To evaluate the reliability of the flood susceptibility map, the Receiver Operating Characteristic (ROC) curve and the Area Under the Curve (AUC) method were applied. This approach is widely acknowledged as a robust and objective means of assessing the predictive performance of spatial models.

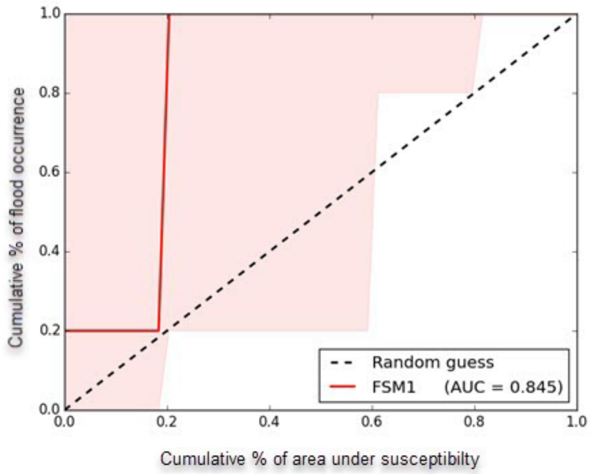

Figure 6. The validation of the Flood Susceptibility Model computed as an AUC.

For validation, 30 historical flood locations were identified through field surveys and historical records to serve as the “positive” dataset, while an equal number of non-flood points were randomly generated in areas known to be safe from inundation. The AUC value quantifies the model’s ability to correctly distinguish between flood-prone and non-flooded zones. In this study, the obtained AUC value was 0.845 (84.5%), as shown in Figure 6. According to standard classification, an AUC value ranging between 0.8 and 0.9 indicates “very good” predictive performance.

This high level of accuracy confirms that the AHP-based model and the selected conditioning factors are effective and reliable tools for predicting flood susceptibility in the Bouarfa watershed. The correspondence between the mapped flood susceptibility zones and actual flood occurrences further demonstrates the efficiency and accuracy of the AHP approach in identifying vulnerable areas. Field investigations were carried out to locate flood-prone sites, determine the causes of past flooding, and assess the condition of hydraulic structures and developments along the watercourses (wadis and tributaries).

The findings revealed that flooding in the city of Bouarfa primarily results from the overflow of key watercourses during heavy rainfall events. Among these, Oued Bouarfa originating in the reliefs of Jbel Bouarfa and Hezem El Ahmar and crossing the eastern part of the city is the most significant, followed by Oued Chegga, which flows from the Bni Guil hills through the western sector. The northern part of the city, including the Ennakhil housing estate and Hay Jbel district, is also affected by several chaâbas (small tributary channels). Despite previous flood protection interventions, the diagnostic field visit confirmed that certain areas remain vulnerable, underlining the need to evaluate the effectiveness of existing measures.

Furthermore, the AUC analysis (Kayastha et al., 2013) substantiates the performance of the AHP model, as the calculated 84.5% response rate reflects a high level of accuracy in simulating flood susceptibility. The cumulative percentage of flood-prone areas plotted in Figure 6 demonstrates the strong correlation between predicted and observed flood locations, confirming the reliability of the adopted methodology for flood risk assessment and management in Bouarfa watershed.

5.3. Discussion and Implications

The flood susceptibility analysis conducted in Bouarfa watershed using the AHP method reveals significant results that warrant in-depth discussion regarding hydrological risk management issues in semi-arid regions of Morocco and the Maghreb. Methodological consistency constitutes a fundamental prerequisite for the reliability of any multi-criteria analysis. In our study, the obtained consistency ratio (CR) of 0.018 is well below the critical threshold of 0.10 established by Saaty (1977, 1980), attesting to the robustness of the weighting of conditioning factors. This value reflects a logical and rigorous hierarchization of criteria, strengthening the scientific validity of our approach. Similar results have been reported by Chihi et al. (2025) in the Jeffara basin in Tunisia, where a consistency ratio of 0.01 was obtained, demonstrating the reproducibility of this method in semi-arid environments of the Maghreb (Chihi et al., 2025).

Validation using the ROC curve and the AUC value of 0.845 (84.5%) confirms the "very good" performance of the model according to international classification standards. This performance is comparable to that obtained by Elhadi et al. (2025) in the city of Souk-Ahras in Algeria, where a hybrid AHP-XGBoost model achieved an AUC of 84.5% (Elhadi et al., 2025). However, it remains inferior to the performances of hybrid machine learning models recently developed in similar contexts. For example, El Haou et al. (2025) obtained an AUC of 92.98% with an RF-SVM model in the semi-arid city of Beni Mellal in Morocco (El Haou et al., 2025), while Bammou et al. (2024) reached an average AUC of 0.93 with the XGBoost algorithm in the Haouz plain of the Moroccan High (Bammou et al., 2024).

Nevertheless, the AHP method presents considerable advantages in data-limited contexts, characteristic of semi-arid regions. As highlighted by Chihi et al. (2025), knowledge-driven approaches integrating geological expertise and local knowledge prove particularly relevant in environments where historical flood data are scarce or incomplete. The transparency and interpretability of AHP also facilitate its appropriation by local decision-makers, unlike the "black boxes" that constitute certain machine learning algorithms. This aspect is crucial for the effective implementation of flood risk management policies in developing countries where technical capacities may be limited.

The spatial distribution of flood susceptibility classes in Bouarfa watershed reveals that more than 60% of the study area (60.47%) is classified under high to very high susceptibility, with 39.46% and 21.01% respectively. These proportions are consistent with observations made in other semi-arid basins of North Africa. Kasri et al. (2023) demonstrated similar vulnerability patterns in Souss watershed in Morocco, where multicriteria analysis in a GIS environment identified significant flood-prone areas concentrated in low-lying zones with high drainage density (Kasri et al., 2023). The convergence of these results across different Maghreb watersheds suggests common hydro-geomorphological characteristics that predispose semi-arid regions to flash flooding.

The concentration of very high susceptibility zones in the central and downstream portions of the watershed, particularly around the city of Bouarfa, highlights the interaction between natural factors and anthropogenic pressures. The low elevation, gentle slopes (0–5°), and endoreic drainage patterns create conditions favorable to water accumulation, while rapid urbanization exacerbates vulnerability by increasing impervious surfaces and modifying natural drainage networks. This urban flood problematic has been extensively documented in similar North African contexts. El Haou et al. (2025) emphasized that rapid urbanization in Beni Mellal, combined with mountainous terrain accelerating water flow, significantly amplifies flood risks in semi-arid urban environments. Similarly, Elhadi et al. (2025) identified high urbanization rates as a major contributing factor to flash floods in Souk-Ahras, Algeria.

Field investigations conducted in this study revealed that flooding in Bouarfa city primarily results from the overflow of key watercourses, notably Oued Bouarfa and Oued Chegga, during intense rainfall events. This finding aligns with the fluvial flood dynamics observed in other Moroccan cities. El Baida et al. (2024) developed a real-time urban flood depth mapping model for the flood-prone city of Zaio in Morocco, demonstrating that flood dynamics influenced by outer watersheds require sophisticated prediction approaches capable of accounting for both pluvial and fluvial components (El Baida et al., 2024). The persistence of vulnerable areas despite previous flood protection interventions in Bouarfa underscores the necessity of comprehensive approaches integrating both structural and non-structural measures.

The implications of our results extend beyond immediate flood risk identification. The susceptibility map provides a strategic tool for regional planning and land-use management, particularly in the context of climate change. Climate projections for North Africa indicate an intensification of extreme precipitation events in semi-arid regions, which could significantly increase flood frequency and magnitude. El Baida et al. (2025) quantified this concern by employing modified Intensity-Duration-Frequency curves adjusted for the RCP8.5 climate scenario in their assessment of nature-based solutions for flood mitigation in Zaio, Morocco (El Baida et al., 2025). Their findings demonstrate that proactive adaptation strategies, including detention ponds, riparian reforestation, and green infrastructure, can achieve substantial flood discharge reductions (28.95% for fluvial floods and 44.7% for pluvial floods) while contributing to water resource preservation in water-scarce regions.

The identification of geological and soil characteristics as critical conditioning factors in our study resonates with recent research emphasizing the importance of subsurface heterogeneity in flood susceptibility modeling. Chihi et al. (2025) argued that geological and structural features should not be merely treated as data inputs but integrated as explanatory drivers to improve spatial prediction accuracy, particularly under data-scarce conditions. Their geology-driven knowledge approach in the Tunisian Jeffara basin achieved an excellent AUC of 96%, validated through multi-event cloud-based analysis using Sentinel-1 imagery. This methodological advancement suggests that future flood susceptibility studies in semi-arid regions could benefit from enhanced integration of geological controls and geostatistical techniques to better represent subsurface processes influencing infiltration, runoff generation, and flood propagation.

The high to very high susceptibility zones identified around Bouarfa city require immediate attention from local authorities for the implementation of targeted mitigation strategies. These findings can inform land-use zoning regulations to restrict new construction in the most vulnerable areas and guide the strategic placement of flood defense structures such as retention basins, levees, and drainage improvement works. Moreover, the development of early warning systems tailored to high-risk communities should be prioritized. The integration of remote sensing and real-time monitoring technologies, as demonstrated by El Baida et al. (2024) with convolutional neural networks achieving 99.17% computational time reduction, offers promising avenues for operational flood forecasting systems in data-scarce environments.

Our results align with the objectives of Morocco's National Water Plan and Water Law 36-15, which emphasize integrated water resource management and the protection of populations and infrastructure from water-related hazards. The flood susceptibility map provides a concrete tool for implementing these policies at the local level, facilitating evidence-based decision-making for flood risk reduction. Furthermore, the methodology employed in this study, combining AHP with GIS and remote sensing, can be transferred to other semi-arid watersheds in Morocco and the Maghreb region facing similar challenges.

Despite the robust performance of the AHP model, certain limitations should be acknowledged. The static nature of the susceptibility map does not account for temporal variability in conditioning factors, particularly land use changes and climate variability. Future research could explore dynamic modeling approaches incorporating temporal datasets to capture evolving flood risks. Additionally, while the AHP method effectively integrates expert knowledge, it remains subjective in factor weighting. Hybrid approaches combining AHP with machine learning algorithms, as successfully implemented by Elhadi et al. (2025) and demonstrated to outperform standalone methods, represent a promising direction for enhancing predictive accuracy while maintaining interpretability. The integration of nature-based solutions within flood management strategies, as advocated by El Baida et al. (2025), should also be explored for the Bouarfa watershed, considering their dual benefits in flood mitigation and water resource conservation in water-stressed semi-arid regions.

6. Conclusion

The flood susceptibility map was developed using the Analytic Hierarchy Process (AHP), a decision-support method that combines expert judgment with quantitative analysis to ensure model consistency. By integrating key conditioning factors such as elevation, slope, drainage density, flow accumulation, land use/land cover (LULC), geology, and soil the study accurately identified flood-prone areas within Bouarfa watershed. Results show that about 60.47% of the basin is exposed to high or very high flood risk, mainly in low-lying plains and gentle slopes near Bouarfa and along the main river channels. Among the seven analyzed factors, slope, elevation, and drainage density were the most influential. The model achieved an AUC value of 0.845 (84.5%), confirming its strong predictive capability. The resulting map serves as a practical tool for planners, engineers, and decision-makers to guide flood mitigation, land-use planning, and emergency response strategies.

Despite these promising results, further measures are needed to reduce flood risks in Bouarfa. Future assessments should consider environmental vulnerability by including agricultural zones, surface water systems, and infrastructure. Urban expansion and land-use decisions must also integrate runoff management and the protection of natural drainage paths. Developing clear criteria for evaluating surface water quality, especially regarding sediment load, is equally important. Additionally, public awareness and training on flood risks and safety measures before, during, and after flood events should be strengthened, in line with Water Law 36-15. The use of high-resolution imagery, such as QuickBird data, would enhance the precision of flood mapping and inventories.

To advance this research, future studies should apply the same methodology to other flood-prone regions and incorporate both temporal and socio-economic dimensions. Using satellite time-series data (e.g., Sentinel-2) would allow monitoring changes in flood susceptibility over time, while integrating information on population density and infrastructure value would help transition from susceptibility mapping to comprehensive risk assessment. Including local knowledge of flood behavior would also improve the model's relevance and community acceptance. Overall, this study provides a solid scientific foundation for sustainable flood management and strengthens the resilience of Bouarfa watershed to future flooding.

Author contributions: Conceptualization, ZEA, AM and ML; methodology, ZEA, AA ; software, ZEA, and SE; validation, ZEA, AM and MM; formal analysis, ZEA; writing—original draft preparation, ZEA; writing—review and editing, ZEA, AM and ML; visualization, ZEA, AA, MS, SE and MM; supervision, AM. All authors have read and agreed to the published version of the manuscript

Conflict of interest: The authors declare no conflict of interest.

7. References

1. Adiat, K. A. N., Nawawi, M. N. M., & Abdullah, K. (2012). Assessing the accuracy of GIS-based elementary multi criteria decision analysis as a spatial prediction tool – A case of predicting potential zones of sustainable groundwater resources. *Journal of Hydrology*, *440–441*, 75–89. https://doi.org/10.1016/j.jhydrol.2012.03.028
2. Bammou, Y., Benzougagh, B., Igmoullan, B., Ouallali, A., Kader, S., Spalevic, V., Sestras, P., Billi, P., & Marković, S. B. (2024). Optimizing flood susceptibility assessment in semi-arid regions using ensemble algorithms: A case study of Moroccan High Atlas. *Natural Hazards*, *120*(8), 7787–7816. https://doi.org/10.1007/s11069-024-06550-z
3. Bates, P. D. (2012). Integrating remote sensing data with flood inundation models: How far have we got? *Hydrological Processes*, *26*(16), 2515–2521. https://doi.org/10.1002/hyp.9374
4. Benito, G., Rico, M., Sánchez-Moya, Y., Sopeña, A., Thorndycraft, V. R., & Barriendos, M. (2010). The impact of late Holocene climatic variability and land use change on the flood hydrology of the Gua-

dalentín River, southeast Spain. *Global and Planetary Change*, *70*(1–4), 53–63. https://doi.org/10.1016/j.gloplacha.2009.11.007

5. Botzen, W. J. W., Aerts, J. C. J. H., & Van Den Bergh, J. C. J. M. (2013). Individual preferences for reducing flood risk to near zero through elevation. *Mitigation and Adaptation Strategies for Global Change*, *18*(2), 229–244. https://doi.org/10.1007/s11027-012-9359-5
6. Chapi, K., Singh, V. P., Shirzadi, A., Shahabi, H., Bui, D. T., Pham, B. T., & Khosravi, K. (2017). A novel hybrid artificial intelligence approach for flood susceptibility assessment. *Environmental Modelling & Software*, *95*, 229–245. https://doi.org/10.1016/j.envsoft.2017.06.012
7. Chihi, H., Hammami, M. A., & Mezni, I. (2025). Flood susceptibility mapping in data-scarce arid environments: Guided by geology-driven knowledge and multi-event cloud-based validation. *Natural Hazards*, *121*(18), 20855–20901. https://doi.org/10.1007/s11069-025-07533-4
8. Choubin, B., Moradi, E., Golshan, M., Adamowski, J., Sajedi-Hosseini, F., & Mosavi, A. (2019). An ensemble prediction of flood susceptibility using multivariate discriminant analysis, classification and regression trees, and support vector machines. *Science of The Total Environment*, *651*, 2087–2096. https://doi.org/10.1016/j.scitotenv.2018.10.064
9. Dahri, N., & Abida, H. (2017). Monte Carlo simulation-aided analytical hierarchy process (AHP) for flood susceptibility mapping in Gabes Basin (southeastern Tunisia). *Environmental Earth Sciences*, *76*(7), 302. https://doi.org/10.1007/s12665-017-6619-4
10. Das, S. (2018). Geographic information system and AHP-based flood hazard zonation of Vaitarna basin, Maharashtra, India. *Arabian Journal of Geosciences*, *11*(19), 576. https://doi.org/10.1007/s12517-018-3933-4
11. Das, S., & Pardeshi, S. D. (2018). Comparative analysis of lineaments extracted from Cartosat, SRTM and ASTER DEM: A study based on four watersheds in Konkan region, India. *Spatial Information Research*, *26*(1), 47–57. https://doi.org/10.1007/s41324-017-0155-x
12. Dewan, A. (2013). *Floods in a Megacity: Geospatial Techniques in Assessing Hazards, Risk and Vulnerability*. Springer Netherlands. https://doi.org/10.1007/978-94-007-5875-9
13. Doocy, S., Daniels, A., Packer, C., Dick, A., & Kirsch, T. D. (2013). The Human Impact of Earthquakes: A Historical Review of Events 1980-2009 and Systematic Literature Review. *PLoS Currents*. https://doi.org/10.1371/currents.dis.67bd14fe457f1db0b5433a8ee20fb833
14. El Baida, M., Boushaba, F., Chourak, M., & Hosni, M. (2024). Real-Time Urban Flood Depth Mapping: Convolutional Neural Networks for Pluvial and Fluvial Flood Emulation. *Water Resources Management*, *38*(12), 4763–4782. https://doi.org/10.1007/s11269-024-03886-w
15. El Baida, M., Chourak, M., & Boushaba, F. (2025). Flood Mitigation and Water Resource Preservation: Hydrodynamic and SWMM Simulations of nature-based Solutions under Climate Change. *Water Resources Management*, *39*(3), 1149–1176. https://doi.org/10.1007/s11269-024-04015-3
16. El Haou, M., Ourribane, M., Keshavarzi, A., Ismaili, M., Eloudi, H., Hajji, S., El Bouzkraoui, M., Namous, M., & Krimissa, S. (2025). Hybrid machine learning models for urban flood susceptibility assessment in semi-arid Beni Mellal, Morocco: A spatial and comparative analysis. *Modeling Earth Systems and Environment*, *11*(6), 403. https://doi.org/10.1007/s40808-025-02584-9
17. Elhadi, M., Sabri, D., Yassine, D., & Yahia, H. (2025). Flash flood risk mapping using analytic hierarchy process and machine learning: Case of Souk-Ahras City, Northeastern Algeria. *Euro-Mediterranean Journal for Environmental Integration*. https://doi.org/10.1007/s41207-025-00885-0
18. Elkhrachy, I. (2015). Flash Flood Hazard Mapping Using Satellite Images and GIS Tools: A case study of Najran City, Kingdom of Saudi Arabia (KSA). *The Egyptian Journal of Remote Sensing and Space Science*, *18*(2), 261–278. https://doi.org/10.1016/j.ejrs.2015.06.007
19. Emerton, R., Cloke, H. L., Stephens, E. M., Zsoter, E., Woolnough, S. J., & Pappenberger, F. (2017). Complex picture for likelihood of ENSO-driven flood hazard. *Nature Communications*, *8*(1), 14796. https://doi.org/10.1038/ncomms14796
20. Fernández, D. S., & Lutz, M. A. (2010). Urban flood hazard zoning in Tucumán Province, Argentina, using GIS and multicriteria decision analysis. *Engineering Geology*, *111*(1–4), 90–98. https://doi.org/10.1016/j.enggeo.2009.12.006
21. García-Ruiz, J. M., Nadal-Romero, E., Lana-Renault, N., & Beguería, S. (2013). Erosion in Mediterranean landscapes: Changes and future challenges. *Geomorphology*, *198*, 20–36. https://doi.org/10.1016/j.geomorph.2013.05.023

22. Haghizadeh, A., Siahkamari, S., Haghiabi, A. H., & Rahmati, O. (2017). Forecasting flood-prone areas using Shannon's entropy model. *Journal of Earth System Science*, *126*(3), 39. https://doi.org/10.1007/s12040-017-0819-x
23. Ibrahim-Bathis, K., & Ahmed, S. A. (2016). Geospatial technology for delineating groundwater potential zones in Doddahalla watershed of Chitradurga district, India. *The Egyptian Journal of Remote Sensing and Space Science*, *19*(2), 223–234. https://doi.org/10.1016/j.ejrs.2016.06.002
24. Kasri, J. E., Lahmili, A., Bouajaj, A., & Soussi, H. (2023). The Application of Remote Sensing and GIS Tools in Mapping of Flood Risk Areas in the Souss Watershed Morocco. In X.-S. Yang, R. S. Sherratt, N. Dey, & A. Joshi (Eds), *Proceedings of Eighth International Congress on Information and Communication Technology* (Vol. 693, pp. 275–295). Springer Nature Singapore. https://doi.org/10.1007/978-981-99-3243-6_22
25. Kayastha, P., Dhital, M. R., & De Smedt, F. (2013). Application of the analytical hierarchy process (AHP) for landslide susceptibility mapping: A case study from the Tinau watershed, west Nepal. *Computers & Geosciences*, *52*, 398–408. https://doi.org/10.1016/j.cageo.2012.11.003
26. Kazakis, N., Kougias, I., & Patsialis, T. (2015). Assessment of flood hazard areas at a regional scale using an index-based approach and Analytical Hierarchy Process: Application in Rhodope–Evros region, Greece. *Science of The Total Environment*, *538*, 555–563. https://doi.org/10.1016/j.scitotenv.2015.08.055
27. Khosravi, K., Nohani, E., Maroufinia, E., & Pourghasemi, H. R. (2016). A GIS-based flood susceptibility assessment and its mapping in Iran: A comparison between frequency ratio and weights-of-evidence bivariate statistical models with multi-criteria decision-making technique. *Natural Hazards*, *83*(2), 947–987. https://doi.org/10.1007/s11069-016-2357-2
28. Kia, M. B., Pirasteh, S., Pradhan, B., Mahmud, A. R., Sulaiman, W. N. A., & Moradi, A. (2012). An artificial neural network model for flood simulation using GIS: Johor River Basin, Malaysia. *Environmental Earth Sciences*, *67*(1), 251–264. https://doi.org/10.1007/s12665-011-1504-z
29. Kourgialas, N. N., & Karatzas, G. P. (2011). Flood management and a GIS modelling method to assess flood-hazard areas—A case study. *Hydrological Sciences Journal*, *56*(2), 212–225. https://doi.org/10.1080/02626667.2011.555836
30. Kumar, S., Raghuwanshi, N. S., & Mishra, A. (2015). Identification and management of critical erosion watersheds for improving reservoir life using hydrological modeling. *Sustainable Water Resources Management*, *1*(1), 57–70. https://doi.org/10.1007/s40899-015-0005-8
31. Leake, C., & Malczewski, J. (2000). GIS and Multicriteria Decision Analysis. *The Journal of the Operational Research Society*, *51*(2), 247. https://doi.org/10.2307/254268
32. Lehner, B., Verdin, K., & Jarvis, A. (2006). *HydroSHEDS Technical Documentation, Version 1.0*. World Wildlife Fund US, Washington, DC.
33. Li, K., Wu, S., Dai, E., & Xu, Z. (2012). Flood loss analysis and quantitative risk assessment in China. *Natural Hazards*, *63*(2), 737–760. https://doi.org/10.1007/s11069-012-0180-y
34. Mahmoud, S. H., & Gan, T. Y. (2018). Multi-criteria approach to develop flood susceptibility maps in arid regions of Middle East. *Journal of Cleaner Production*, *196*, 216–229. https://doi.org/10.1016/j.jclepro.2018.06.047
35. Malczewski, J. (2006). GIS-based multicriteria decision analysis: A survey of the literature. *International Journal of Geographical Information Science*, *20*(7), 703–726. https://doi.org/10.1080/13658810600661508
36. Merz, B., Kreibich, H., Schwarze, R., & Thieken, A. (2010). Review article "Assessment of economic flood damage" *Natural Hazards and Earth System Sciences*, *10*(8), 1697–1724. https://doi.org/10.5194/nhess-10-1697-2010
37. Norman, L. M., Huth, H., Levick, L., Shea Burns, I., Phillip Guertin, D., Lara-Valencia, F., & Semmens, D. (2010). Flood hazard awareness and hydrologic modelling at Ambos Nogales, United States–Mexico border. *Journal of Flood Risk Management*, *3*(2), 151–165. https://doi.org/10.1111/j.1753-318X.2010.01066.x
38. Oeurng, C., Sauvage, S., & Sánchez-Pérez, J.-M. (2011). Assessment of hydrology, sediment and particulate organic carbon yield in a large agricultural catchment using the SWAT model. *Journal of Hydrology*, *401*(3–4), 145–153. https://doi.org/10.1016/j.jhydrol.2011.02.017
39. Onuşluel Gül, G. (2013). Estimating flood exposure potentials in Turkish catchments through index-based flood mapping. *Natural Hazards*, *69*(1), 403–423. https://doi.org/10.1007/s11069-013-0717-8
40. Pradhan, B., Shafiee, M., & Pirasteh, S. (2009). Maximum flood prone area mapping using RADARSAT images and GIS: kelantan river basin. *Int. J.Geoinformatics*, *5*(2), 13.

41. Rahmati, O., Zeinivand, H., & Besharat, M. (2016). Flood hazard zoning in Yasooj region, Iran, using GIS and multi-criteria decision analysis. *Geomatics, Natural Hazards and Risk*, *7*(3), 1000–1017. https://doi.org/10.1080/19475705.2015.1045043
42. Saaty, T. L. (1977). A scaling method for priorities in hierarchical structures. *Journal of Mathematical Psychology*, *15*(3), 234–281. https://doi.org/10.1016/0022-2496(77)90033-5
43. Saaty, T. L. (1980). The Analytic Hierarchy Process. *McGraw-Hill New York.*
44. Saaty, T. L., & Vargas, L. G. (2012). *Models, Methods, Concepts & Applications of the Analytic Hierarchy Process* (Vol. 175). Springer US. https://doi.org/10.1007/978-1-4614-3597-6
45. Samanta, S., Koloa, C., Kumar Pal, D., & Palsamanta, B. (2016). Flood Risk Analysis in Lower Part of Markham River Based on Multi-Criteria Decision Approach (MCDA). *Hydrology*, *3*(3), 29. https://doi.org/10.3390/hydrology3030029
46. Stieglitz, M., Rind, D., Famiglietti, J., & Rosenzweig, C. (1997). An Efficient Approach to Modeling the Topographic Control of Surface Hydrology for Regional and Global Climate Modeling. *Journal of Climate*, *10*(1), 118–137. https://doi.org/10.1175/1520-0442(1997)010%253C0118:AEATMT%253E2.0.CO;2
47. Tehrany, M. S., Pradhan, B., & Jebur, M. N. (2013). Spatial prediction of flood susceptible areas using rule based decision tree (DT) and a novel ensemble bivariate and multivariate statistical models in GIS. *Journal of Hydrology*, *504*, 69–79. https://doi.org/10.1016/j.jhydrol.2013.09.034
48. Tehrany, M. S., Pradhan, B., & Jebur, M. N. (2015). Flood susceptibility analysis and its verification using a novel ensemble support vector machine and frequency ratio method. *Stochastic Environmental Research and Risk Assessment*, *29*(4), 1149–1165. https://doi.org/10.1007/s00477-015-1021-9
49. Vojtek, M., & Vojteková, J. (2019). Flood Susceptibility Mapping on a National Scale in Slovakia Using the Analytical Hierarchy Process. *Water*, *11*(2), 364. https://doi.org/10.3390/w11020364
50. Youssef, A. M., Pradhan, B., & Hassan, A. M. (2011). Flash flood risk estimation along the St. Katherine road, southern Sinai, Egypt using GIS based morphometry and satellite imagery. *Environmental Earth Sciences*, *62*(3), 611–623. https://doi.org/10.1007/s12665-010-0551-1
51. Zhao, G., Pang, B., Xu, Z., Yue, J., & Tu, T. (2018). Mapping flood susceptibility in mountainous areas on a national scale in China. *Science of The Total Environment*, *615*, 1133–1142. https://doi.org/10.1016/j.scitotenv.2017.10.037